WILEY-VCH

RESEARCH ARTICLE

Benchmark Dynamics of Dipolar Molecular Rotors in Fluorinated Metal-Organic Frameworks

Jacopo Perego,[a] Charl X. Bezuidenhout,[a] Silvia Bracco,[a],* Sergio Piva,[a] Giacomo Prando,[b],* Cristian Aloisi,[b] Pietro Carretta,[b] Jiří Kaleta,[c],* Thi Phuong Le,[c] Piero Sozzani,[a] Andrea Daolio[a] and Angiolina Comotti[a],*

[a] Dr. J. Perego, Dr. C. X. Bezuidenhout, Prof. S. Bracco, Dr. S. Piva, Dr. A. Daolio, Prof. P. Sozzani, Prof. A. Comotti
Department of Materials Science, University of Milano - Bicocca, Via R. Cozzi 55, 20125 Milan, Italy.
E-mail: angiolina.comotti@unimib.it, silvia.bracco@unimib.it

[b] Dr. G. Prando, C. Aloisi, Prof. P. Carretta,
Department of Physics, University of Pavia, Via Bassi 6, 27100 Pavia, Italy.
E-mail: giacomo.prando@unipv.it

[c] Prof. J. Kaleta, T. P. Le
Institute of Organic Chemistry and Biochemistry, Czech Academy of Sciences, Flemingovo náměstí 542/2, 16000, Prague, Czech Republic.
Email: jiri.kaleta@uochb.cas.cz

Supporting information for this article is given via a link at the end of the document.

Abstract: Fluorinated Metal-Organic Frameworks (MOFs), comprising a wheel-shaped ligand with geminal rotating fluorine atoms, produced benchmark mobility of correlated dipolar rotors at 2 K, with practically null activation energy (E_a = 17 cal/mol). ^{1}H T_1 NMR revealed multiple relaxation phenomena due to the exchange among correlated dipole-rotor configurations. Synchrotron radiation X-ray diffraction at 4 K, Density Functional Theory, Molecular Dynamics and phonon calculations showed the fluid landscape and pointed out a cascade mechanism converting dipole configurations into each other. Gas accessibility, shown by hyperpolarized-Xe NMR, allowed for chemical stimuli intervention: CO_2 triggered dipole reorientation, reducing their collective dynamics and stimulating a dipole configuration change in the crystal. Dynamic materials under limited thermal noise and high responsiveness enable the fabrication of molecular machines with low energy dissipation and controllable dynamics.

Introduction

The issue of dynamics in solid materials is growing exponentially and comprises stimulating achievements in the fabrication of molecular switches, motors and rotors.[1-12] The synergy among these areas promotes a beneficial circulation of concepts addressed to ensure facile molecular reorientation and responsiveness to external stimuli. This, in turn, can be translated into tailored materials with functional properties, including the transformation of light into a useful molecular movement which drives, for instance, gas absorption on command.[13-18] Furthermore, dielectric and optical properties and switchable ferroelectricity become accessible.[19-21] In particular, attractive functional properties can be activated by incorporating fast-reorientable dipoles onto molecular rotors to produce materials responsive to static or oscillating electric fields.[22-25] However, the integration of dipolar groups in place of simple apolar ones into struts of the designed material, yet preserving the overall integrity of the architecture and fast-rotor response, may encounter obstacles caused by long-range Coulombic interactions among dipoles and their larger steric encumbrance (e.g. C-F *vs* C-H), which may restrict dynamics.[25,26] These undesired constraints can be attenuated or opportunely tuned by keeping dipoles apart, owing to the design and construction of porous materials with large free volumes.[27-29] Indeed, porous materials can promote motion without disrupting the basic design of the overall architecture.[30,31] We selected MOFs, crystalline structures that, together with other families of porous compounds, such as Porous Organic Polymers (POPs), Periodic Mesoporous Organosilicas (PMOs) and Porous Molecular Crystals (PMCs),[32-38] have been used for supporting fast group-reorientation in the solid state.[31,39-44]

In this work, we tailored benchmark dipole rotation in MOFs by the rational choice of ligands that could function as struts and hyper-fast dipolar rotors. In our design, we selected a bicyclopentanedicarboxylate rotating wheel and its asymmetrically substituted analogue bearing CF_2 dipoles to fabricate two isostructural Al-MOFs (Al-FTR and Al-FTR-F2, named Frustrated Trigonal Rotor). They exhibited remarkable dynamics down to 2 K, even in the presence of cooperative dipole motion. Synchrotron-source powder X-ray diffraction (PXRD) unveiled the structural behaviour over a wide temperature range down to 4 K. Motional properties were specifically addressed by ^{1}H T_1 NMR relaxation times down to temperatures as low as 2 K and phonon calculations to demonstrate the exceptionally fast reorientation of rotor-mounted CF_2 groups and the extremely low activation energies for dipole rotation. Such a large motional freedom is reminiscent of the liquid state mobility, although the designed material overcomes liquid-phase properties such as motion coherence and the wide temperature range of existence since extremely low temperatures are inaccessible to conventional liquids. Notably, the mobility in Al-FTR-F2, especially in the 2-10 K temperature range, is due to the presence of a concerted dance of dipoles triggered by the interactions among nearest-neighbour rotors. This was demonstrated by Plane-Wave Density Functional Theory (PW-DFT) and Molecular Dynamics, which displayed a sophisticated cascade mechanism of the dipolar rotors and the interconversion among the lowest energy crystal configurations. Quadrupolar CO_2 molecules entering the nano-galleries induce a coherence switch of dipolar rotors, drastically affecting the configuration landscape. Overall,

this work demonstrates a successful design to promote fast dipole mobility in solid matter in an intriguingly fluid energy landscape, even with substantial depliction of thermal agitation, and paves the way to conceive molecular machines with an easy response to chemical and physical stimuli in the solid state.[45]

Results and Discussion

Two MOFs, Al-FTR and its fluorinated analogue Al-FTR-F2, were prepared by self-assembly of the respective ligands, bicyclo[1.1.1]pentane-1,3-dicarboxylate (BCP) and 2,2-difluorobicyclo[1.1.1]pentane-1,3-dicarboxylate (BCP-F2)[46] with Al (III) ions under hydrothermal conditions (Figure 1A and ESI). The crystalline powders, after solvent exchange with methanol, were activated at 130°C under high vacuum to remove any solvent molecules hosted in the structure, thus generating permanently porous materials.[47]

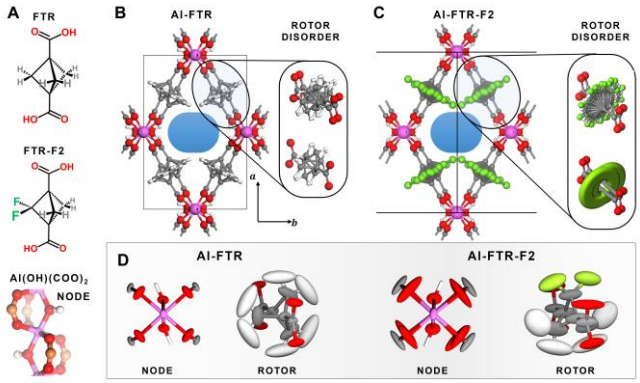

Figure 1. A) Chemical structures of bicyclo[1.1.1]pentane-1,3-dicarboxylic acid and 2,2-difluorobicyclo[1.1.1]pentane-1,3-dicarboxylic acid and the geometry of the Al-node. Crystal structures of Al-FTR (B) and Al-FTR-F2 (C) as viewed along the *c*-axis. In the insets, methylene units of bicyclopentane moieties are disordered over 2 sites in Al-FTR and 4 sites in Al-FTR-F2. D) The thermal ellipsoids for the $Al(OH)(COO)_2$ nodes as well as the FTR and FTR-F2 rotors in both MOFs are reported, as derived from PW-DFT Phonon calculations. The ellipsoids are displayed with a 95% probability factor. Atom labeling: hydrogen = white, carbon = gray, oxygen = red, fluorine = green, aluminum = purple.

The C=O stretching bands in infrared spectroscopy at 1588 cm^{-1} and 1604 cm^{-1} for BCP and BCP-F2 in the MOF structures (compared to 1664 cm^{-1} and 1704 cm^{-1}, respectively, in the free carboxylic acid) indicated the coordination of the ligands to the Al (III) ions. The thermal stability up to 343°C and 323°C for Al-FTR and Al-FTR-F2, respectively, was asserted by thermogravimetric analysis (Figure S8). The PXRD patterns from a synchrotron source, collected from room temperature (RT) to 4 K, identified highly ordered crystalline porous materials with disorder localized on the ligands. At room temperature, the crystal structures were refined in the orthorhombic crystal system with the *Imam* space group for both Al-FTR and Al-FTR-F2. The Al-FTR and Al-FTR-F2 can be described as isoreticular MOF structures with a **sra** net.[48] They are comprised of infinite columns of corner-sharing $AlO_4(OH)_2$ octahedra interconnected by the carboxylate groups of BCP-based ligands, which are arranged perpendicular to the propagation direction of the columns. As viewed down the *c*-axis, the structure shows a rhombus-like connectivity which produces a *trellis-like* structure, typical of these types of Al-MOFs (Figure 1B, 1C, S19 and S20).[49,50]

In the crystal structure of Al-FTR, applying the 6-fold rotational potential of the ligand,[51] the three methylene groups of the bicyclopentane moieties were modelled and refined with disorder over two sites (occupation factor of 0.5) and lie on a plane as a wheel mounted on the main molecular axis (Figure 1B). For Al-FTR-F2, comprising geminal fluorine substituted bicyclopentane moieties, the C_3 axial symmetry of the central wheel is suppressed, generating an asymmetry in the plane of the wheel and orientational disorder (Figure 1C). In Al-FTR, the distances between the hydrogen atoms of neighboring rotors are 2.5-2.7 Å, which are larger than the sum of van der Waals radii (2.4 Å), thus suggesting the revolution is sterically unhindered. In Al-FTR-F2, the steric encumbrance is asymmetrically distributed about the wheel for the presence of fluorine atoms, which generate more severe steric requirements during the rotation owing to $CF_2 \cdots CF_2$ collisions, whilst $CH_2 \cdots CH_2$ and $CH_2 \cdots CF_2$ interactions are allowed, suggesting the occurrence of correlated motion.

A "trampoline-like" disorder was used to model the dicarboxylate ligands for both MOFs, displacing their rotor axis over two positions within the *a-b* plane (Figures 1B and 1C), as informed by PW-DFT phonon calculations (Figures S19 and S20). The atomic thermal displacements are visualized as thermal ellipsoids (Figure 1D). Notably, large thermal ellipsoids are observed both for CH_2 and CF_2 moieties, generating almost circular shapes which suggest rotational dynamics of the ligands.

The 3D frameworks exhibit one-dimensional channels running parallel to the *c*-axis. The channels, as explored using a probe sphere of 1.2 Å radius, show a squeezed rhombus-like cross-section of 4.5 × 5.9 $Å^2$ for Al-FTR and a more rounded 5.0 × 5.7 $Å^2$ cross-section for Al-FTR-F2 (Figure 1, blue area). The channels of the MOFs can accommodate spheres with a maximum diameter of 4.5 Å and 4.9 Å for Al-FTR-F2 and Al-FTR, respectively. Accessibility to gases of the two MOFs was experimentally shown by N_2 adsorption isotherms at 77 K that displayed Langmuir surface areas of 520 $m^2\ g^{-1}$ and 412 $m^2\ g^{-1}$ for Al-FTR and Al-FTR-F2, respectively, with a pore size distribution centred at 6.3 Å, in agreement with the pore size obtained from the crystal structures (Figure 2A and S23). The sudden increase of N_2 uptake at p/p°=0.1 is likely due to the flexible character of the framework.[48] The excellent CO_2 uptake was proven by sorption isotherms at 195 K, yielding an amount adsorbed of 4.0 MPU and 4.2 MPU at 0.2 p/p° for Al-FTR and AL-FTR-F2, respectively (Figure 2B). At very low pressure (p/p° < 0.01), the CO_2 uptake in the fluorinated MOF is higher, indicating a larger affinity of CO_2 with the polar walls. Indeed, *in situ* microcalorimetry coupled with CO_2 adsorption isotherm[52] performed at 293 K proved the higher adsorption enthalpy of -30 kJ/mol for Al-FTR-F2 than that of non-fluorinated analogue (-27 kJ/mol) (Figures 2C and 2D), suggesting specific CO_2 interactions with dipolar rotors, as described later.

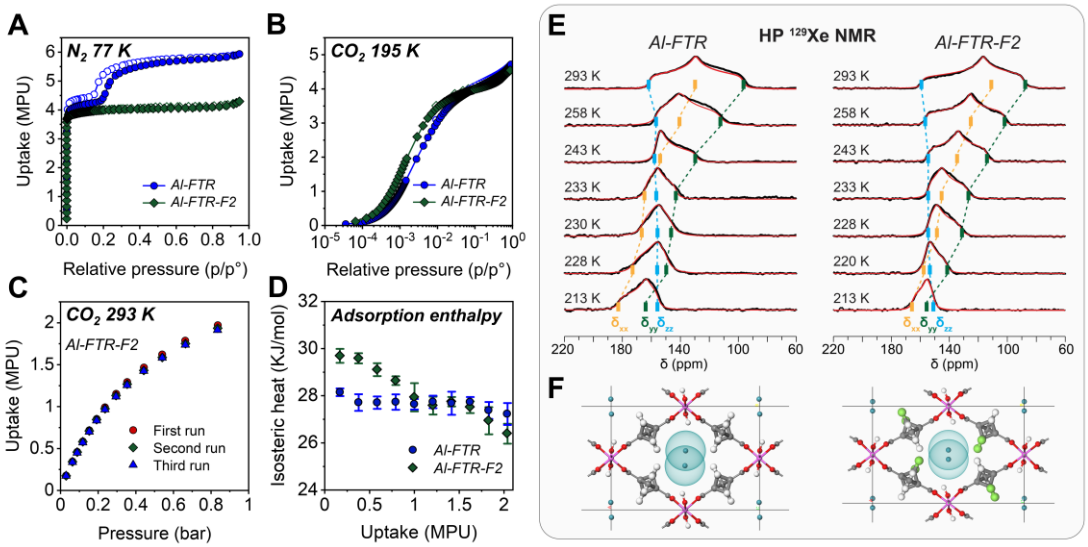

Figure 2. A) N_2 adsorption isotherms measured at 77 K of Al-FTR (blue circles) and Al-FTR-F2 (green diamonds). B) CO_2 adsorption isotherms measured at 195 K of Al-FTR (blue circles) and Al-FTR-F2 (green diamonds). The logarithmic scale highlights the higher uptake of Al-FTR-F2 at low pressure. C-D) CO_2 adsorption isotherms collected simultaneously to microcalorimetric analysis of Al-FTR-F2 and CO_2 adsorption enthalpy of Al-FTR and Al-FTR-F2 as a function of gas uptake. E) Hyperpolarized ^{129}Xe NMR spectra of Al-FTR (left) and Al-FTR-F2 (right), showing the main components of the tensors (δ_{xx}, δ_{yy} and δ_{zz}). Experimental (black lines) and simulated spectra (red lines). F) Arrangement of Xe atoms in the channels: Xe atoms are distributed over two equivalent sites with equal occupancy at distances of 1.6 Å and 0.6 Å for Al-FTR and Al-FTR-F2, respectively.

The laser-assisted hyperpolarized ^{129}Xe NMR directly probed the empty spaces that surround the rotors in the low-density architectures (Figures 2E).[53-56] At 293 K, the pattern of Al-FTR-F2 exhibits a remarkable chemical shift anisotropy CSA with non-axial symmetry, indicating the exploration of an ellipsoidal channel cross-section, as observed in the rhombohedral structure of the framework. The tensor components (δ_{xx} and δ_{yy}) drift downfield in parallel upon lowering the temperature, demonstrating increasing interactions between xenon atoms and the rotors. Al-FTR shows similar behaviour even though the tensor component values are shifted to higher temperatures, indicating a higher affinity of xenon towards the walls. Interestingly, the intense ^{129}Xe NMR signal, detected within 200 ms of Xe diffusion (2% concentration in a He/N_2 mixture) into the frameworks, demonstrated that the channels are guest-free and easily available from the gas phase. Grand Canonical Monte Carlo and PW-DFT *ab-initio* calculations show xenon atoms distributed over two equivalent sites about 0.6 and 1.6 Å apart, for Al-FTR-F2 and Al-FTR respectively (Figure 2F), further supporting the diversified ellipsoidal cross-sections.

Variable temperature PXRD measurements were performed on both MOFs using synchrotron radiation from room temperature down to 4 K. From the unit cell axes, as obtained by Pawley refinement (ESI), the long and short diagonals of the rhombus (*a*- and *b*-axis, respectively) as well as the rotor-rotor center-to-center distances (denoted ***d1*** and ***d2***) as a function of temperature were determined (Figure 3A, 3B). From RT to 75 K, the short rhombus diagonal (*b*-axis) and the rotor-rotor distance ***d2*** for both Al-FTR and Al-FTR-F2 change at the same rate, whilst the ***d1*** distance, which is related to the c-axis, remains constant (Figure 3C).

Below 75 K, for Al-FTR, a continuous change of the ***d2*** is observed down to 4 K, with no indication of a plateau. The model for Al-FTR at 4 K shows that the closest inter-rotor distances between the methylene hydrogens (Figure 3D: H···H 2.4 – 2.5 Å) exceed the sum of their van der Waals radii, indicating that there is enough clearance for the molecular rotors to move freely. Regarding Al-FTR-F2, the rotor-rotor distance ***d2*** plateaus at 6.2 Å, unveiling that the dipolar rotors come into van der Waals contact (Figure 3C, 3D) and two CF_2 groups on neighbouring rotors cannot outrun each other. Consequently, these results suggest that a concerted motion is required for rotation.

To solve the crystal structure at 4 K, we considered the possible arrangements of the CF_2 dipoles as determined by the combination of molecular mechanics and PW-DFT (ESI). Rietveld refinement was performed by considering the lowest energy optimized structures which differ in the orientation of their CF_2 dipoles within the rotor layers, as depicted in Figure 3E. At such low temperatures, the trampoline-like mechanism is no longer active, ensuring a stable framework for the rotor motion.

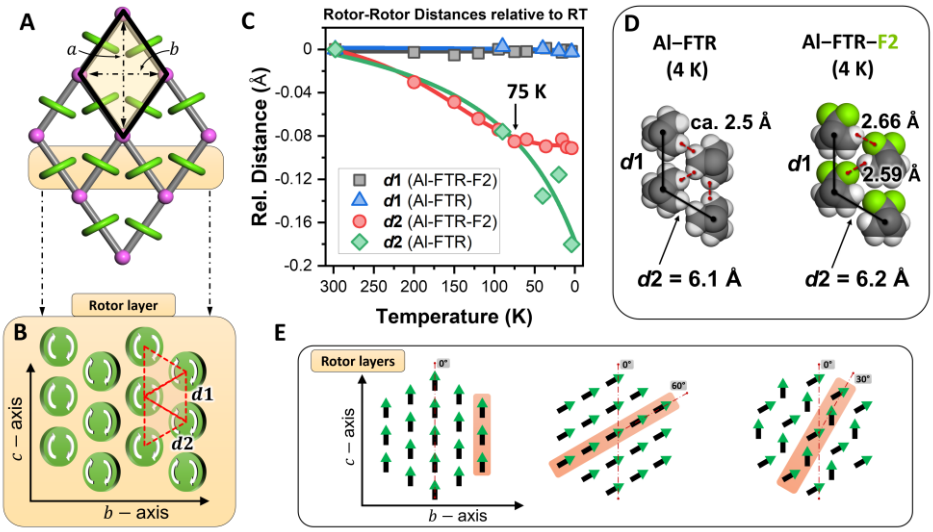

Figure 3. A) Crystal structures, viewed along the *c*-axis, of Al-FTR and Al-FTR-F2 with the characteristic rhombus unit highlighted and its diagonals indicated (long diagonal = *a*-axis, short diagonal = *b*-axis). The nodes are shown in pink spheres, the ligand connectivity in grey sticks and the rotors in green disks. B) Rotor arrangement viewed along the *a*-axis with the trigonal packing is highlighted, and the two unique rotor-rotor distances ***d*1** and ***d*2** are indicated. C) The rotor-rotor distances ***d*1** and ***d*2** (with respect to their values at RT) as a function of temperature from RT down to 4 K, as obtained by Pawley refinement of variable temperature PXRD collected at the ESRF using a synchrotron source. D) The rotor-rotor short-contact distances for the Al-FTR and Al-FTR-F2 for the crystal structures refined by PXRD patterns at 4 K. E) The arrangement of dipolar rotors in the lowest energies crystal structures. The dipolar rotor orientation is illustrated by arrows: the arrowheads represent the fluorine atoms. The orange boxes highlight head-to-tail columns of rotors for easier visualization. Crystal structures either contain anti-parallel layers of rotors or anti-parallel rotor columns, and the net dipole moment for all the structures is zero.

^{1}H T_1 spin-lattice NMR relaxation times are an invaluable source of information to depict the internal dynamics of a material. Measurements have been performed by operating at a few distinct magnetic fields (from 28 to 57 MHz) and exploring a wide temperature range from 298 K to 2 K (Figure 4). According to the Kubo-Tomita function, which correlates the relaxation rates with correlation times as a function of temperature, the fastest relaxation rate is reached when molecular dynamics match the observation frequency (ESI, p. 9).[57]

At the observation frequencies of 28 MHz, the relaxation profile as a function of temperature for Al-FTR reveals a single peak with a maximum at a temperature as low as 16 K, and no further efficient relaxation pathways were detected, suggesting that all motional mechanisms are activated already at low temperatures (Figure 4A).

This is consistent with the presence of a single rotor in the asymmetric unit of the unit cell with ultra-fast dynamics of 3 $*10^7$ Hz at 16 K and a low energy barrier of 237 cal/mol. The attempt frequencies $\tau_0^{-1} = 5*10^{11}$ s^{-1} at infinite temperature appear to agree with the inertial momentum of the rotating mass of 42 g/mol.[58]

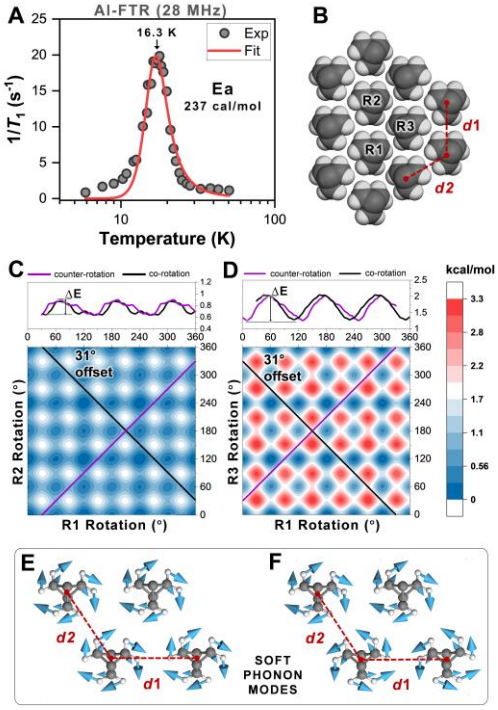

Figure 4. A) ^{1}H $1/T_1$ relaxation rates as a function of temperature at a magnetic field of 28 MHz. The data is fitted with a single component Kubo-Tomita function yielding an E_a of 237 cal/mol at 16.3 K. B) Representation of the model used for the 2D DFT potential energy scans. 2D contour maps with the rotation of rotors pairs R**1** and R**2** (C) and R**1** and R**3** (D) on the X- and Y-axes. The colour scale indicates the ΔE, ranging from 0 kcal/mol (blue) to 3.3 kcal/mol (red). The lines indicate the most optimal co-rotating (R_{co}) and counter-rotating ($R_{counter}$) pathways on the energy surfaces, with the relative rotor rotational offset indicated for each. The ΔE plot for the most optimal mechanisms of rotations (top). The softest rotary phonon modes as calculated by PW-DFT with frequencies of 20 cm^{-1} (E) and 12 cm^{-1} (F). The blue arrows indicate the displacement vectors and the rotation direction of the rotary vibration. Each of the two modes has a duplicate with the rotary modes in the opposite rotational direction.

2D DFT potential energy scans of two rotating pairs of rotors (R1-R2 and R1-R3), as arranged in the crystal structure, allowed the evaluation of the lowest energy barriers of the preferential pathways (Figures 4B-D and ESI). The average energy barrier for the rotary motion of the two couples of rotors is found to be 240 cal/mol, corresponding to the experimental barrier derived from the fit of the ^{1}H relaxation data. From the phonon calculations of Al-FTR we can identify the phonon modes with longer wavelengths (vibrational mode) which are active even at very low temperatures (Figure 4E). Four phonon modes, that are combinations of *co*-rotating and *counter*-rotating motions at frequencies of 12 cm^{-1} and 20 cm^{-1}, imply that the rotors of Al-FTR can still be rotating at very low temperatures.

^{1}H T_1 NMR relaxation profile of Al-FTR-F2 at 22 MHz shows an articulated dynamical behaviour, which exhibits multiple phenomena covering a wide range of temperatures (Figure 5A). Seven Kubo-Tomita functions allowed for an excellent fitting of the profile. Activation energies E_a higher than 100 cal/mol (E_a = 143, 214, 429, 743 and 1542 cal/mol) and attempt frequencies extrapolated to infinite temperature τ_0^{-1} from 2*10^{9} s^{-1} to 3*10^{10} s^{-1} were determined for functions which display maximum relaxation rates between 16 K and 154 K. At the lowest temperature limits, additional relaxation phenomena were found with two on-resonance maxima at 3.6 K and 6.9 K, suggesting that the dipolar rotors explore exceptional re-orientational rates as fast as 2*10^{7} Hz at such low temperatures. Activation energies as low as 17 cal/mol and 41 cal/mol are the benchmarks in the field of dipolar rotors and in the lowest energy limit for molecular rotors, only comparable to BCP rotors in MOFs, such as in Zn-FTR (6 cal mol^{-1})[9] and FTR-P1 (24 cal mol^{-1})[51] and bicyclo-octane-based (BCO) rotors in Zn-MOF (185 cal mol^{-1}).[41] Examples of correlated rotors in crystalline solids yielded activation energy barriers higher than 1 kcal mol^{-1}, as studied by variable temperature solid-state NMR and dielectric spectroscopy.[28,59,60] The attempt frequencies τ_0^{-1} of 3 and 6*10^{8} s^{-1} are clearly below the theoretical value calculated from the inertial mass of a single rotor (≈ 10^{12} s^{-1}), indicating the occurrence of correlated motion within domains of CF2-dipoles (Figures S60 and S61).

DFT calculations show that a single rotor in the most stable structures experiences a high barrier for a complete rotation (Figures 6B and S58 and S59). In fact, the absolute maxima of the profile represent the severe energy requirements occurring for unfavourable interactions of fluorine atoms with those of neighbouring rotors. However, in the profile, lower barriers for 60° reorientations appear, which account for a rapid rotation; thus, a complete rotation with low energy barriers is made possible only by correlated mechanisms which involve several rotors.

Molecular dynamics simulation highlights the rotation mechanism of a rotor collection with the conversion among rotor configurations (Figures 6C, S60, S61 and see Video_1 and Video_2). Interestingly, the conversion occurs spontaneously through a cascade mechanism that involves a long sequence of interacting rotors in series with a 60° reorientation of each rotor and a low activation energy (Figure S63). Steps of each rotor during the cascade are sketched in Figure 6D. Successive cascade events enable the transformation among the structures, realizing a 360° rotation of rotors (Figure S64). Thus, the unusual effect of easy-reorientable dipolar rotors at very cold temperatures and with virtually negligible activation energies, as observed by ^{1}H T_1, can be ascribed to cooperative motion that involves the interconversion among the lowest energy structures. This mechanism is particularly relevant since any dipole reorientation is expected to be frozen under such extreme conditions, except for rare examples such as methyl groups with low molecular masses.[61] At higher temperatures, the thermal agitation promotes the exploration of rotary mechanisms with higher activation energies and less correlated motion. Furthermore, phonon calculations show frequency modes of the dipolar rotators as low as 30 - 39 cm^{-1}. Additionally, the main frequency modes associated with the framework, such as twisting and trampoline, which interfere with the rotator motion, show higher energies (60 - 79 cm^{-1}) (Figure S20). Therefore, at very low temperatures, the stable framework on which the main axis of the rotors is pivoted also favours the impressive rotary dynamics observed for these dipolar rotors.

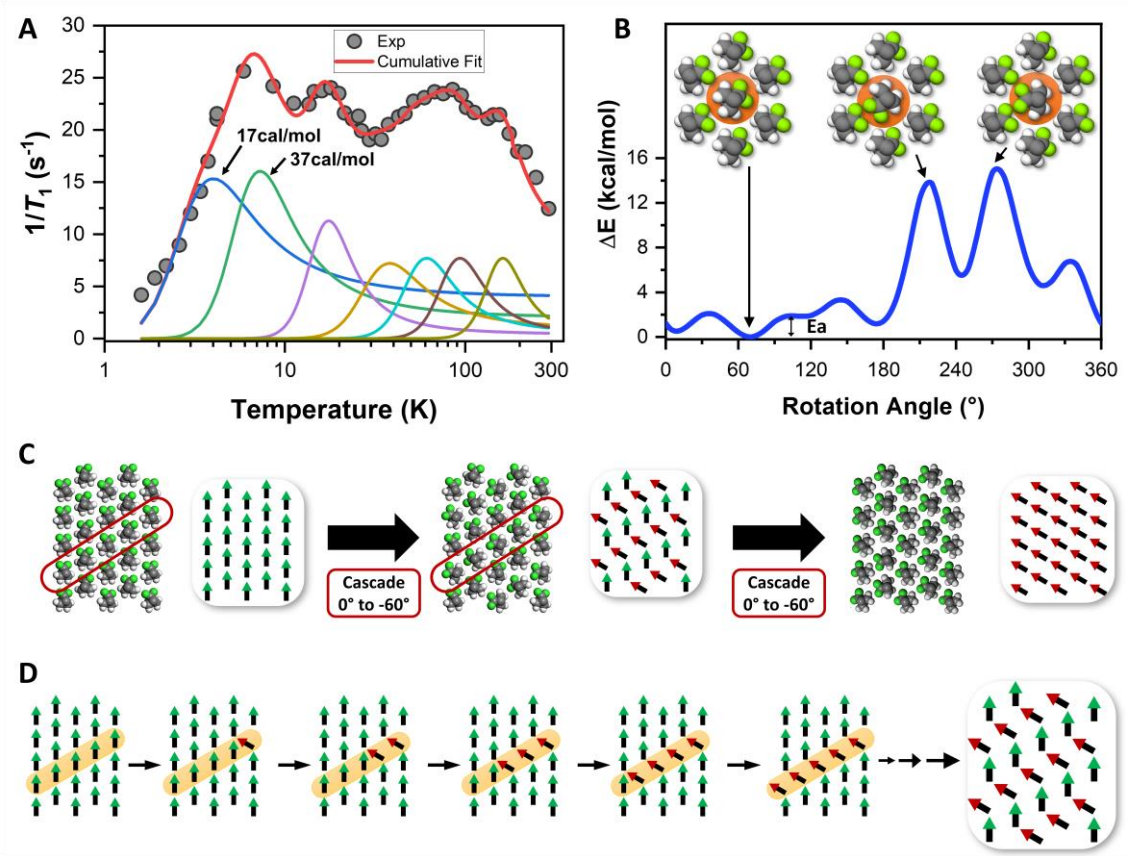

Figure 5. A) ^{1}H 1/T$_1$ relaxation rates of Al-FTR-F2 at 22 MHz fitted using seven Kubo-Tomita functions. The grey circles indicate the experimental data, while the lines represent the fitting curves. The activation energies (E$_a$) are indicated for the two extreme temperatures. B) The single rotor scan computed using DFT for a rotor within the arrangement of structure 3. The global minima and two adjacent barriers are indicated as well as the configurations at selected positions along the scan pathway. C) Snapshots of a molecular-dynamics simulation showing structures in succession at various stages of the simulation. D) Representation of the rotor layers, showing the stepwise cascade mechanism of a row of rotors. The reoriented rotors are shown with red arrowheads for clarity. The yellow box highlights the row involved in a cascade reorientation of rotors.

The dipolar rotors are permanently exposed towards the channels of the porous material, as previously demonstrated by PXRD and HP ^{129}Xe NMR. To move a step forward and show the active intervention of chemical species, which can thus interact with rotor dipoles, Al-FTR-F2 was loaded with CO_2 at the constant pressure of 2.5 bar, PXRD patterns were collected from RT down to 213 K (Figure 6A,6B and Table S12). Below 250 K, the *a*-axis starts shrinking while the *b*-axis expands, unveiling the structural breathing and reorganization of dipolar rotors stimulated by the CO_2 occupation in the cavities. At 213 K and 2.5 bar, full loading is reached at 4 CO_2 molecules per unit cell, in agreement with the CO_2 isotherm at 195 K and p/p° = 0.62. CO_2 molecules are arranged with their main axis perpendicular to the channel axis (Figure 6C). Remarkably, intermolecular interactions between CO_2 electropositive carbon and electronegative fluorine atoms in the rotor and between CO_2 oxygens and rotor hydrogens explain the gymnastic of the rhombohedral shape due to the reorientation of the rotors about CO_2. In fact, the favourable interactions of rotor with CO_2, while exploring the new energy landscape, overcome the rotor-rotor interactions of the empty structure. This is a rare case of a crystal which contains such supramolecular fluorine - carbon dioxide interactions in a stable association. [62-64]

A further feature of interest is that, unconventionally, a switch in dipole configuration is induced in the porous crystal upon gas intervention, suggesting a reorganization of the structure (Figure 6D), and a considerable hampering of dipolar rotor dynamics. However, the ultimate demonstration of motion quenching, caused by CO_2 loading, was achieved by very short spin-lattice relaxation rates (1/T$_1$), measured in the temperature range from 20 to 300 K. The inefficient relaxation and the disappearance of the multiple fast-relaxing phenomena observed in the free-pore sample is indicative of a less dynamic structure. Indeed, under gas pressure of 3 bar, much slower ^{1}H 1/T$_1$ relaxation rates (^{1}H T$_1$=3-5 s for CO_2 loaded sample and 0.04-0.5 s for the empty sample at 57 MHz) as a function of temperature are detected without any apparent maxima, indicating a rather rigid structure, in sharp contrast with the porous sample recorded under vacuum (Figure 6E). This experiment has the relevant implication that the hyper-mobile collective phenomena with extremely low energy barriers can exist only in the absence of any species in the channels, since diffused-in species interacting with the rotors interrupt the continuity of the correlated dipole chains and switch off the delicate motional mechanism. Moreover, the minimal interactions of dipolar rotors at very low temperatures can be controlled by external stimuli, even with gases, and generate amplified effects, opening stimulating perspectives for the modulation of the global properties of the materials.

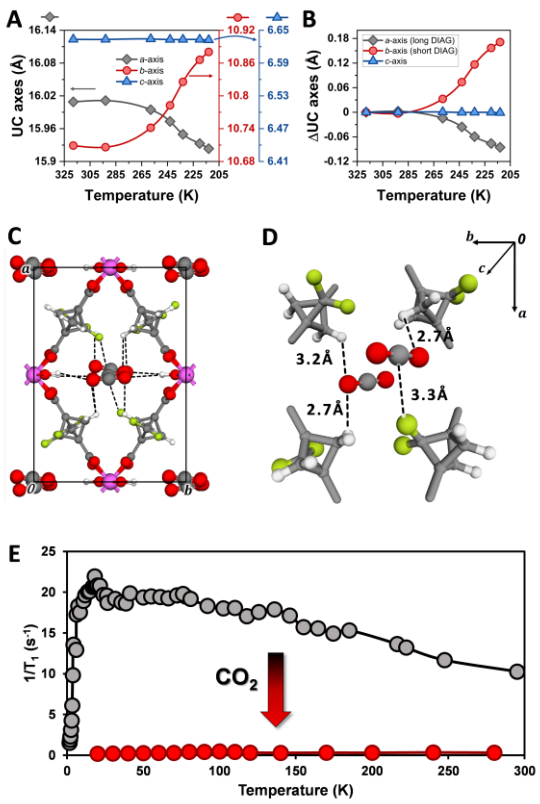

Figure 6. A) Unit-cell parameters obtained by Pawley refinement of VT-PXRD collected under 2.5 bar CO_2 from RT down to 213 K for Al-FTR-F2. B) Changes in the unit-cell axes with respect to the RT unit cell. C – D) The CO_2-loaded Al-FTR-F2 structure using the 213 K unit-cell and optimized by PW-DFT. The black dashed line indicates the short contacts made by the CO_2 molecule. The relevant CO_2–host distances are indicated and noted. E) ^1H $1/T_1$ vs temperature of Al-FTR-F2 (grey circles) and loaded-CO_2 Al-FTR-F2 (red circles) at 57 MHz.

Conclusion

Our endeavour was the construction of isostructural porous Al-MOFs and the in-depth investigation of fluorine atoms as asymmetrically substituted onto the rotating wheels in the solid state. To our surprise, the rotating wheels bearing CF_2 dipoles were endowed with exceptional mobility persistent down to very low temperatures of 2 K. The inter-rotor dipole-dipole interaction between CF_2 groups creates a concerted dance of the dipoles mounted on the hypermobile rotors, leading to a very energy-inexpensive correlated mechanism. The measurement of energy for rotation of the dipolar system was only 17 cal/mol, which is a benchmark value, indicative of the extreme ease of dipole reorientation (10^7 Hz at 4 K). Multiple higher energy barriers are explored at intermediate temperatures, as shown by ^1H T_1 NMR, and explained by *ab-initio* DFT and molecular dynamics simulations. Such motional phenomena of dipoles demonstrate the feasibility of unusual dipolar materials with liquid-regime mobility that are still dynamically active at temperatures prohibitive for motion in solids. The use of such fast-responsive properties opens new windows for applications in sensing, switching, the translation of light irradiation into movement, and the control of solid-state dynamics with external electric fields minimizing energy dissipation.

Acknowledgements

J.P. and C.X.B. contributed equally.
Financial support from the Italian Ministry of University and Research (MIUR) through the grant 'Dipartimenti di Eccellenza-2017 Materials For Energy' is acknowledged. This research was funded by the PRIN NEMO-20173L7W8K and SHERPA-2020EZ8EPB grants. We are grateful to the ESRF synchrotron facility in Grenoble (France) for access to the ID22 beamline (Project: HC-4781) and to O.G.Grendal for technical support. S.B. thanks Lombardy Region for the "Enhancing Photosynthesis" Award and J.P. University of Milano Bicocca for the "Giovani Talenti" Award. T.P.L. and J.K. greatly appreciate the financial support from the Institute of Organic Chemistry and Biochemistry of the Czech Academy of Sciences (RVO: 61388963) and the Czech Science Foundation (grant number: 20-13745S).

Data Availability Statement

The data that support the findings of this study are available in the supplementary material of this article.

Keywords: Metal Organic Frameworks • Molecular Dynamics • Molecular Rotor • Fluorine • Crystal Engineering

[1] S. Krause, B. L. Feringa, *Nat. Rev. Chem.* **2020**, *4*, 550–562.
[2] D. Sluysmans, J. F. Stoddart, *Proc. Natl. Acad. Sci. U. S. A.* **2018**, *115*, 9359−9361.
[3] J.-P. Collin, C. Dietrich-Buchecker, P. Gaviña, M. C. Jimenez-Molero, J.-P. Sauvage, *Acc. Chem. Res.* **2001**, *34*, 477−487.
[4] K. Kinbara, T. Aida, *Chem. Rev.* **2005**, *105*, 1377−1400.
[5] P. Martinez-Bulit, A. J. Stirk, S. J. Loeb, *Trends Chem.* **2019**, *1*, 588-600.
[6] A. Coskun, M. Banaszak, R. D. Astumian, J. F. Stoddart, B. A. Grzybowski, *Chem. Soc. Rev.* **2012**, *41*, 19-30.
[7] M. Baroncini, S. Silvi, A. Credi, *Chem. Rev.* **2020**, *120*, 200−268
[8] J. Michl, E. Charles, H. Sykes, *ACS Nano* **2009**, *3*, 1042-1048.
[9] J. Perego, S. Bracco, M. Negroni, C. X. Bezuidenhout, G. Prando, P. Carretta, A. Comotti, P. Sozzani, *Nat. Chem.* **2020**, *12*, 845-851.
[10] G. Prando, J. Perego, M. Negroni, M. Riccò, S. Bracco, A. Comotti, P. Sozzani, P. Carretta, *Nano Lett.* **2020**, *20*, 7613–7618.
[11] J. Kaleta, J. Chen, G. Bastien, M. Dračínský, M. Mašát, C. T. Rogers, B. L. Feringa, J. Michl, *J. Am. Chem. Soc.* **2017**, *139*, 10486-10498.
[12] C. Santos Hurtado, G. Bastien, M. Mašát, J. R. Štoček, M. Dračínský, I. Rončević, I. Císařová, C. T. Rogers, J. Kaleta, *J. Am. Chem. Soc.* ***2020**, 142, 9337-9351.*
[13] F. Castiglioni, W. Danowski, J. Perego, F. King-Chi Leung, P. Sozzani, S. Bracco, S. J. Wezenberg, A. Comotti, B. L. Feringa, *Nat. Chem.* **2020**, *12*, 595-602.
[14] M. Baroncini, S: d'Agostino, G. Bergamini, P. Ceroni, A. Comotti, P. Sozzani, I. Bassanetti, F. Grepioni, T. M. Hernandez, S. Silvi, M. Venturi, A. Credi, *Nat. Chem.* **2015**, *7*, 634-640.
[15] N. Yanai, T. Uemura, M. Inoue, R. Matsuda, T. Fukushima, M. Tsujimoto, S. Isoda, S. Kitagawa, *J. Am. Chem. Soc.* **2012**, *134*, 4501-4504.

[16] R. Lyndon, K. Konstas, B. P. Ladewig, P. D. Southon, C. J. Kepert, M. R. Hill, *Angew. Chem. Int. Ed.* **2013**, *52*, 3695-3698.

[17] F. Bigdeli, C. T. Lollar, A. Morsali, H.-C. Zhou, *Angew. Chem. Int. Ed.* **2020**, *59*, 4652-4669.

[18] J. Kaleta, G. Bastien, J. Wen, M. Dračínský, E. Tortorici, I. Císařová, P. D. Beale, C. T. Rogers, J. Michl, *J. Org. Chem.* ***2019****, 84,* 8449-8467.

[19] S. Kassem, T. van Leeuwen, A. S. Lubbe, M. R. Wilson, B. L. Feringa, D. A. Leigh, *Chem. Soc. Rev.* **2017**, *46*, 2592−2621.

[20] A. S. Tayi, A. Kaeser, M. Matsumoto, T. Aida, S. I. Stupp, *Nat. Chem.* **2015**, *7*, 281-294.

[21] J. Neumann, K. E. Gottschalk, R. D. Astumian, *ACS Nano* **2012***, 6*, 5242-5248.

[22] W. Danowski, F. Castiglioni, A. S. Sardjan, S. Krause, L. Pfeifer, D. Roke, A. Comotti, W. R. Browne, B. L. Feringa, *J. Am. Chem. Soc.* **2020**, *142*, 9048-9056.

[23] J. Vacek, J. Michl, *Proc. Natl Acad. Sci. USA* **2001**, *98*, 5481–5486.

[24] J. Vacek, J. Michl, *Adv. Funct. Mater.* **2007**, *17*, 730-739.

[25] A. Rodríguez-Fortea, J. Kaleta, C. Méziècre, M. Allain, E. Canadell, P. Wzietek, J. Michl, P. Batail, *ACS Omega* ***2018****, 3, 1293-1297.*

[26] J. Kaleta, J. Michl, C. Mézière, S. Simonov, L. Zorina, P. Wzietek, A. Rodríguez-Fortea, E. Canadell, P. Batail, *CrystEngComm* ***2015****, 17, 7829-7834.*

[27] S. Bracco, M. Beretta, A. Cattaneo, A. Comotti, A. Falqui, K. Zhao, C. Rogers, P. Sozzani, *Angew. Chem. Int. Ed.* **2015**, *54*, 4773 –4777

[28] Y.-S. Su, E. S. Lamb, I. Liepuoniute, A. Chronister, A. L. Stanton, P. Guzman, S. Pérez-Estrada, T. Y. Chang, K. N. Houk, M. A. Garcia-Garibay, S. E. Brown, *Nat. Chem.* **2021**, *13*, 278-283.

[29] L. Kobr, Ke Zhao, Y. Shen, A. Comotti, S. Bracco, R. K. Shoemaker, P. Sozzani, N. A. Clark, J. C. Price, C. T. Rogers, J. Michl, *J. Am. Chem. Soc.* **2012**, *134*, 24, 10122–10131.

[30] J. Dong, V. Wee, S. Bo Peh, D. Zhao, *Angew. Chem. Int. Ed.* **2021**, *60*, 16279–16292.

[31] A. Comotti, S. Bracco, P. Sozzani, *Acc. Chem. Res.* **2016**, *49*, 1701−1710.

[32] O. M. Yaghi, M. J. Kalmutzki, C. S. Diercks, in *Introduction to Reticular Chemistry: Metal-Organic Frameworks and Covalent Organic Frameworks*. Wiley-VCH, Germany **2019**.

[33] S. Das, P. Heasman, T. Ben, S. Qiu, *Chem. Rev.* **2017**, *117*, 1515-1563.

[34] S. Inagaki, S. Guan, T. Ohsuna, O. Terasaki, *Nature* **2002**, *416*, 304-307.

[35] J.-B. Lin, T. TT Nguyen, R. Vaidhyanathan, J. Burner, J. M. Taylor, H. Durekova, F. Akhtar, R. K. Mah, O. Ghaffari-Nik, S. Marx, N. Fylstra, S. S. Iremonger, K. W. Dawson, P. Sarkar, P. Hovington, A. Rajendran, T. K Woo, G. K. H. Shimizu, *Science* **2021**, *374*, 1464-1469.

[36] I. Bassanetti, S. Bracco, A. Comotti, M. Negroni, C. Bezuidenhout, S. Canossa, P. P. Mazzeo, L. Marchiò, P. Sozzani, *J. Mater. Chem. A* **2018**, *6*, 14231-14239.

[37] G. Xing, I. Bassanetti, S. Bracco, M. Negroni, C. Bezuidenhout, T. Ben, P. Sozzani, A. Comotti, *Chem. Sci.* **2019**, *10*, 730-736.

[38] I. Bassanetti, A. Comotti, P. Sozzani, S. Bracco, G. Calestani, F. Mezzadri, L. Marchio, *J. Am. Chem. Soc.* **2014**, *136*, 14883-14895.

[39] M. Inukai, T. Fukushima, Y. Hijikata, N. Ogiwara, S. Horike, S. Kitagawa, *J. Am. Chem. Soc.* **2015**, *137*, 38, 12183–12186.

[40] A. Comotti, S. Bracco, T. Ben, S. Qiu, P. Sozzani, *Angew. Chem. Int. Ed.* **2014**, *53*, 1043-1047.

[41] C. S. Vogelsberg, F. J. Uribe-Romo, A. S. Lipton, S. Yang, K. N. Houk, S. Brown, M. A. Garcia-Garibay, *Proc. Nat. Ac. Sci.* **2017**, *114*, 13613-13618.

[42] A. Comotti, S. Bracco, A. Yamamoto, M. Beretta, T. Hirukawa, N. Tohnai, M. Miyata, P. Sozzani, *J. Am. Chem. Soc.* **2014**, *136*, 618−621.

[43] A. Comotti, S. Bracco, P. Valsesia, M. Beretta, P. Sozzani, *Angew. Chem. Int. Ed.* **2010**, *49*, 1760-1764.

[44] C. S Vogelsberg, S. Bracco, M. Beretta, A. Comotti, P. Sozzani, M. A Garcia-Garibay, *J. Phys. Chem. B* **2012**, *116*, 1623-1632.

[45] L. Feng, R. D. Astumian, J. F. Stoddart, *Nat. Rev. Chem.* **2022**, *6* , 705-725.

[46] Le, T. P.; Rončević, I.; Dračínský, M.; Císařová, I.; Šolínová, V.; Kašička, V.; Kaleta, J. *J. Org. Chem.* **2021**, *86*, 10303-10319.

[47] Deposition numbers 2194587 (for activated Al-FTR, phase 1), 2194588 (for activated Al-FTR, phase 2), 2194589 (for activated Al-FTR-F2, phase 1) and 2194590 (for activated Al-FTR-F2, phase 2) contain the supplementary crystallographic data for this paper. These data are provided free of charge by the joint Cambridge Crystallographic Data Centre and Fachinformationszentrum Karlsruhe Access Structures service.

[48] N. L. Rosi, J. Kim, M. Eddaoudi, B. Chen, M. O'Keeffe, O. M. Yaghi, *J. Am. Chem. Soc.* **2005**, *127*, 1504-1518.

[49] T. Loiseau, C. Serre, C. Huguenard, G. Fink, F. Taulelle, M. Henry, T. Bataille, G. Férey *Chem. Eur. J.* **2004**, *10*, 1373-1382.

[50] A. Comotti, S. Bracco, P. Sozzani, S. Horike, R. Matsuda, J. Chen, M. Takata, Y. Kubota, S. Kitagawa, *J. Am. Chem. Soc.* **2008**, *130*, 13664-13672.

[51] J. Perego, C. X. Bezuidenhout, S. Bracco, G. Prando, L. Marchio', M. Negroni, P. Carretta, P. Sozzani, A. Comotti, *J. Am. Chem. Soc.* **2021**, *143*, 13082-13090.

[52] W. K. Feldmann, K.-A. White, C. X. Bezuidenhout, V. J. Smith, C. Esterhuysen and L. J. Barbour, *ChemSusChem* **2020**, *13*, 102-105.

[53] *Hyperpolarized Xenon-129 Magnetic Resonance: Concepts, Production, Techniques and Applications (New Developments in NMR*, Vol. 2 (Eds: R. Meersmann, E. Brunner), RSC, London, **2015.**

[54] P Sozzani, A Comotti, R Simonutti, T Meersmann, J. W. Logan, A Pines, *Angew. Chem. Int. Ed.* **2000**, *39*, 2695-2699.

[55] A. Comotti, S. Bracco, L. Ferretti M. Mauri, R. Simonutti, P. Sozzani, *Chem. Commun.* **2007**, 350–352.

[56] C. J. Jameson, A. C. de Dios, Xe nuclear magnetic resonance line shapes in nanochannels. *J. Chem. Phys.* **2002**, *116*, 3805-3821.

[57] R. Kubo, K. Tomita, *J. Phys. Soc. Jpn* **1954**, *9*, 888-919.

[58] N. L. Owen in *Internal rotation in molecules*, Wiley monographs in Chemical Physics, Wiley-Interscience, **1974**, 157.

[59] C. Lemouchi, K. Iliopoulos, L. Zorina, S. Simonov, P. Wzietek, T. Cauchy, A. Rodríguez-Fortea, E. Canadell, J. Kaleta, J. Michl, D. Gindre, M. Chrysos, P. Batail, *J. Am. Chem. Soc.* **2013**, *135*, 9366−9376.

[60] I. Liepuoniute, M. J. Jellen, M. A. Garcia-Garibay, *Chem. Sci.* **2020**, *11*, 12994–13007.

[61] K. Eibl, R. Kannengießer, W. Stahl, H. V. L. Nguyen, I. Kleiner, *Molecular Phys.* **2016***, 114*, 3483–3489.

[62] P. Nugent, Y. Belmabkhout, S. D. Burd, A. J. Cairns, R. Luebke, K. Forrest, T. Pham, S. Ma, B. Space, L. Wojtas, M. Eddaoudi, M. J. Zaworotko, *Nature* **2013**, *495*, 80-84.

[63] P. M. Bhatt, Y. Belmabkhout, A. Cadiau, K. Adil, O. Shekhah, A. Shkurenko, L. J. Barbour, M. Eddaoudi, *J. Am. Chem. Soc.* **2016**, *138*, 9301−9307.

[64] A. Pedrini, J. Perego, S. Bracco, C. X. Bezuidenhout, P. Sozzani, A. Comotti, *J. Mater Chem A* **2021**, *9*, 27353-27360.

Entry for the Table of Contents

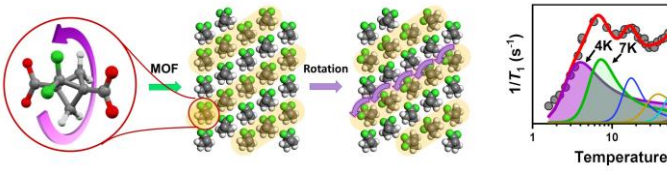

Al-MOF, constructed with a wheelshaped ligand containing geminal rotating fluorine atoms shows a fluid configuration landscape in crystals, even at 2K. The multiple configuration interchange, arising from a correlated cascade mechanism, runs through the structure, as shown by Molecular-Dynamics, phonon calculations and NMR relaxations that occur even at temperatures that usually prohibit any dipole rotation.

Video 1

Click here to access/download

Supporting Information

Video_1 Dyn150K-1 Layer.mp4

Video 2

Click here to access/download

Supporting Information

Video_2 Dyn150K-2 Layers.mp4

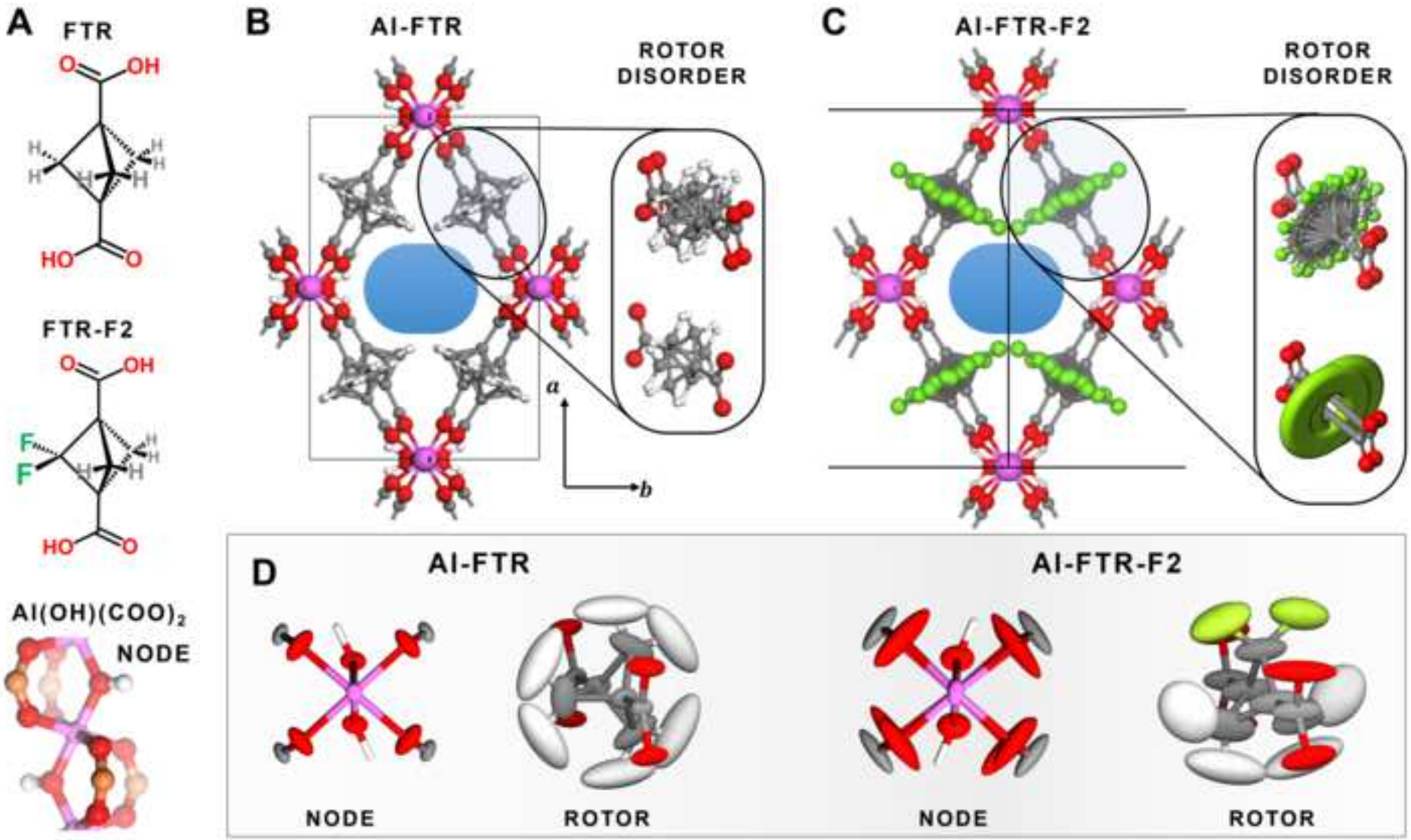

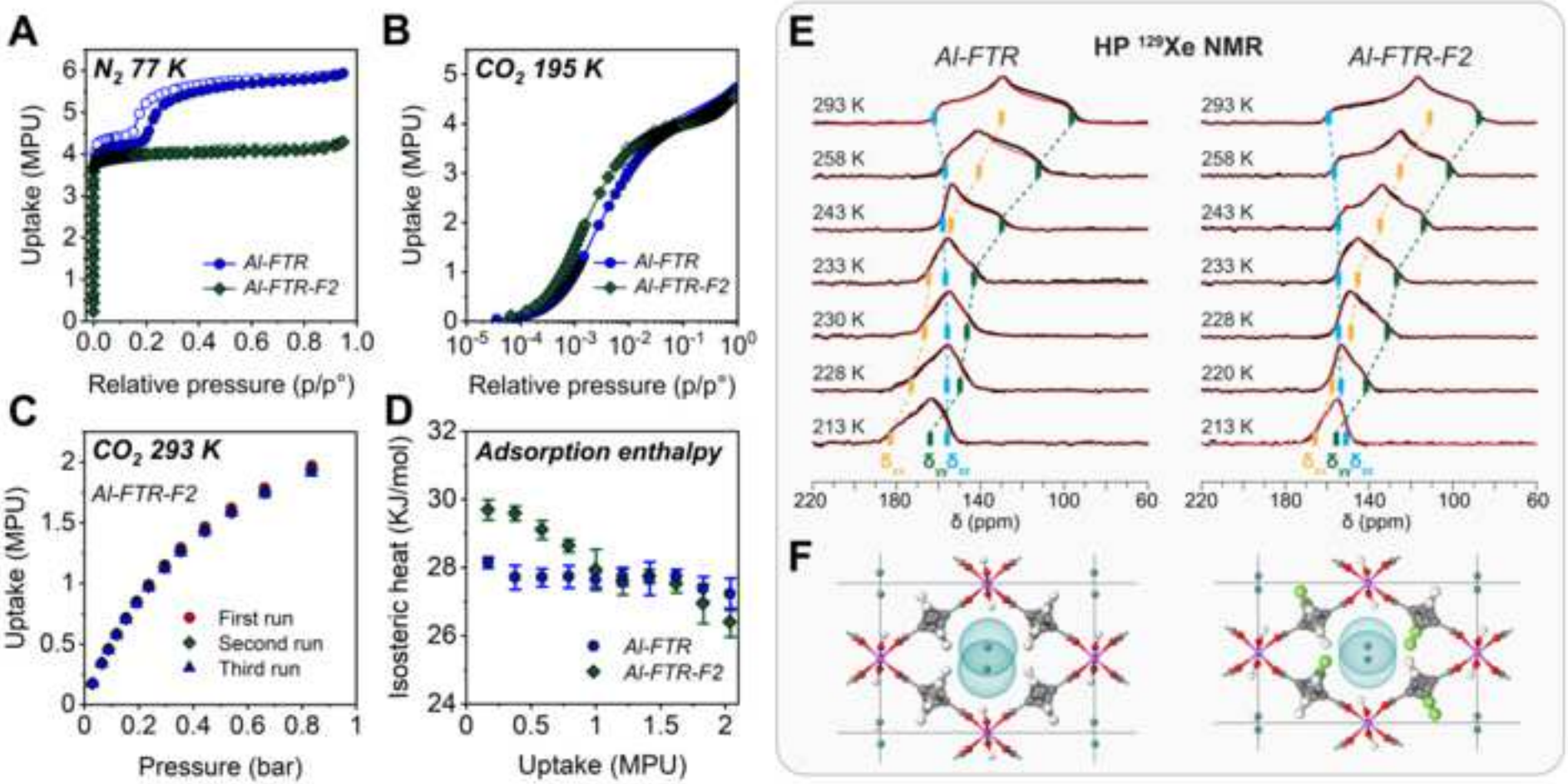

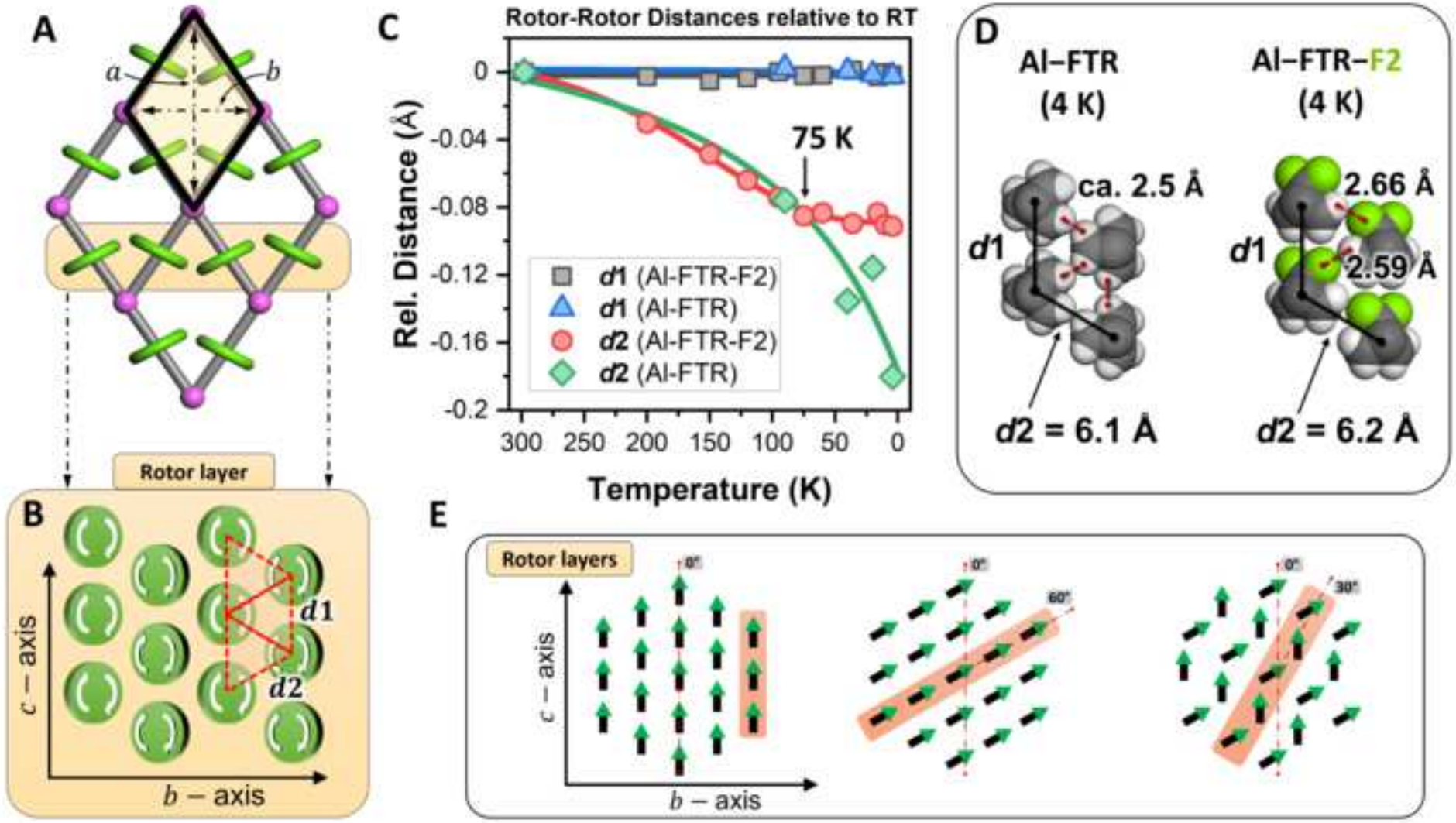
A
a
b
Rotor layer
B
d1
d2
c – axis
b – axis
C
Rotor-Rotor Distances relative to RT
Rel. Distance (Å)
0
-0.04
-0.08
-0.12
-0.16
-0.2
75 K
d1 (Al-FTR-F2)
d1 (Al-FTR)
d2 (Al-FTR-F2)
d2 (Al-FTR)
300 250 200 150 100 50 0
Temperature (K)
D
Al–FTR
(4 K)
ca. 2.5 Å
d1
d2 = 6.1 Å
Al–FTR–F2
(4 K)
2.66 Å
d1
2.59 Å
d2 = 6.2 Å
E
Rotor layers
0°
60°
30°
c – axis
b – axis

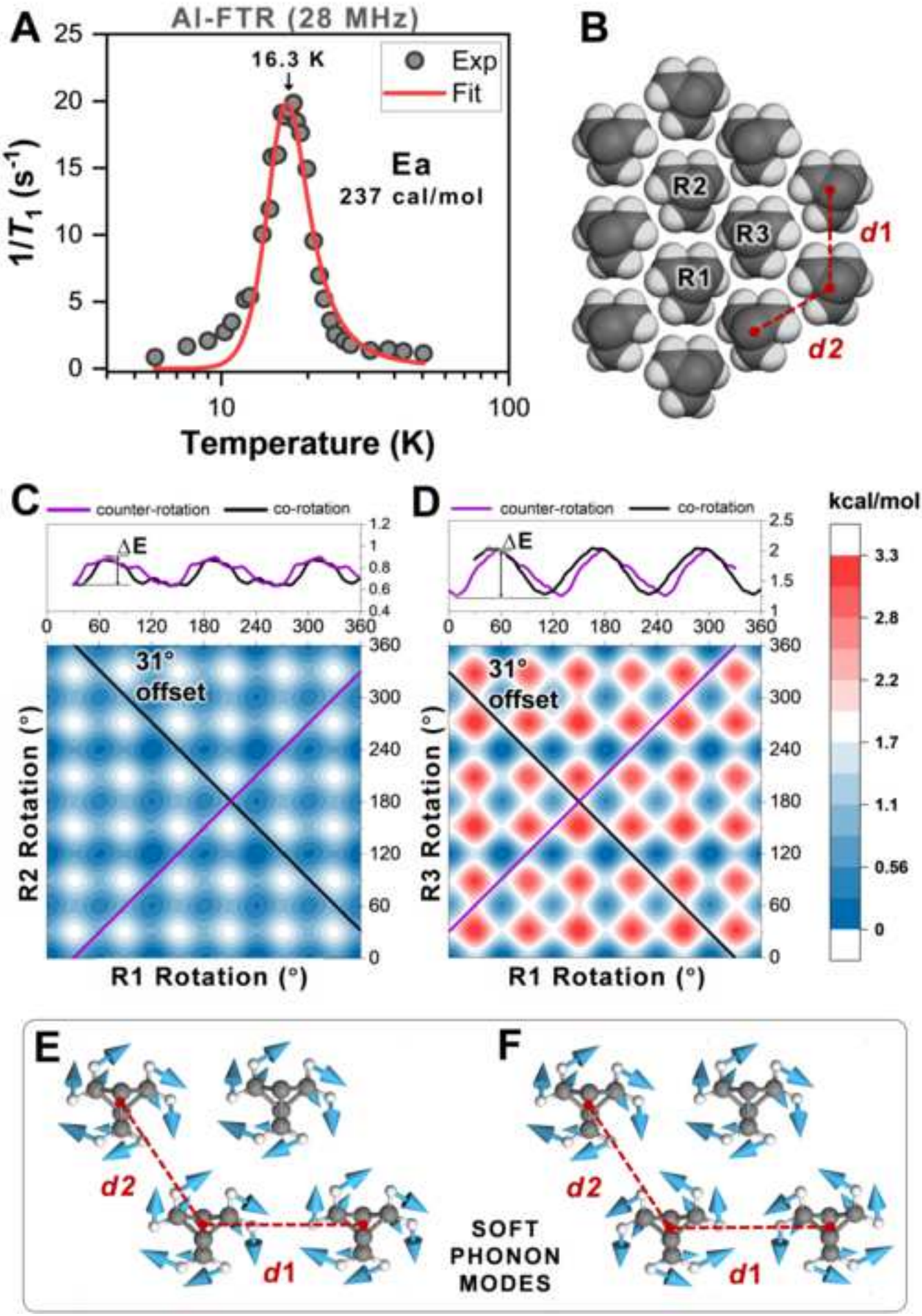
A
Al-FTR (28 MHz)
16.3 K
Exp
Fit
Ea
237 cal/mol
1/T1 (s-1)
Temperature (K)
B
R2
R3
R1
d1
d2
C
counter-rotation
co-rotation
ΔE
31° offset
R2 Rotation (°)
R1 Rotation (°)
D
counter-rotation
co-rotation
ΔE
31° offset
R3 Rotation (°)
R1 Rotation (°)
kcal/mol
3.3
2.8
2.2
1.7
1.1
0.56
0
E
d2
d1
SOFT PHONON MODES
F
d2
d1

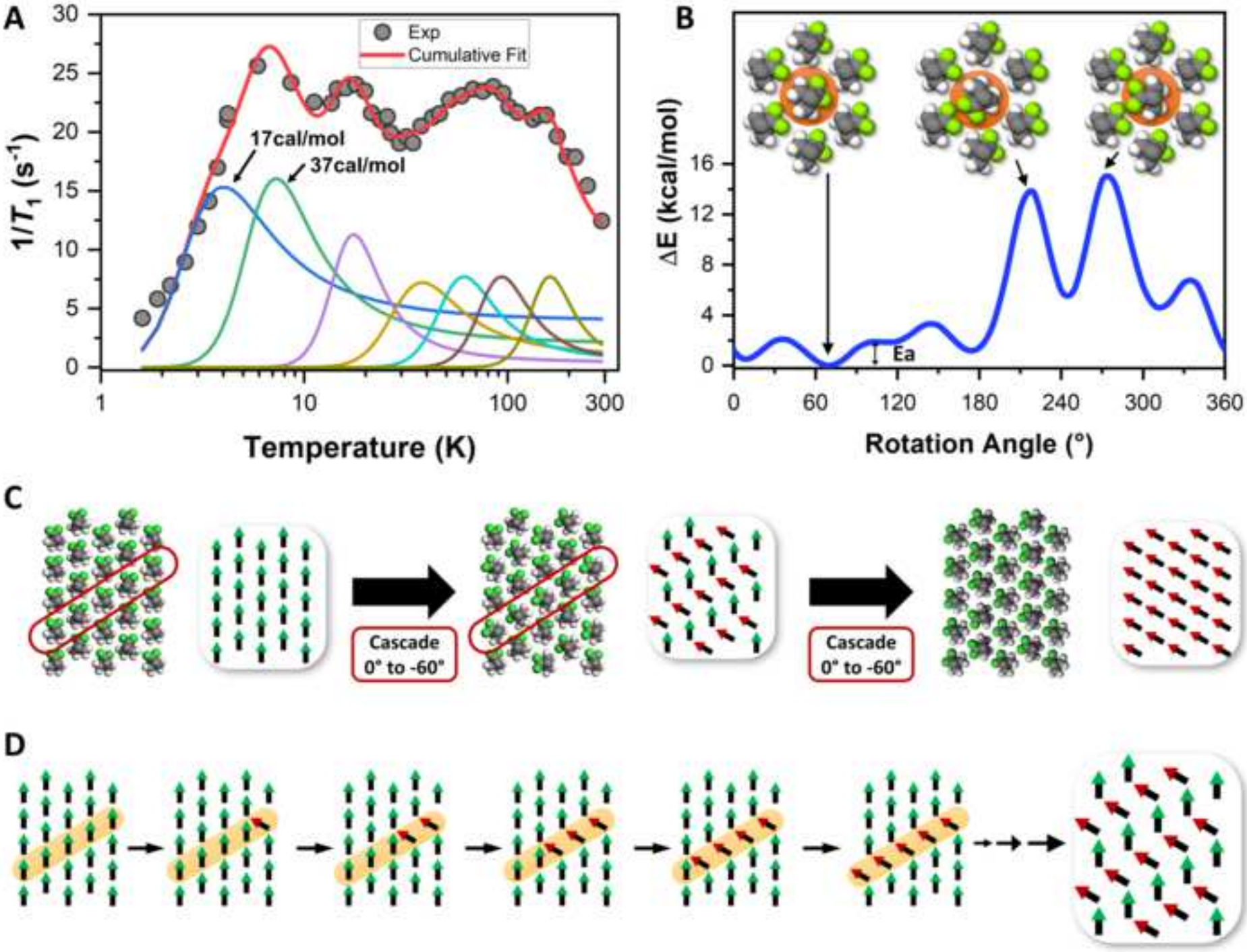

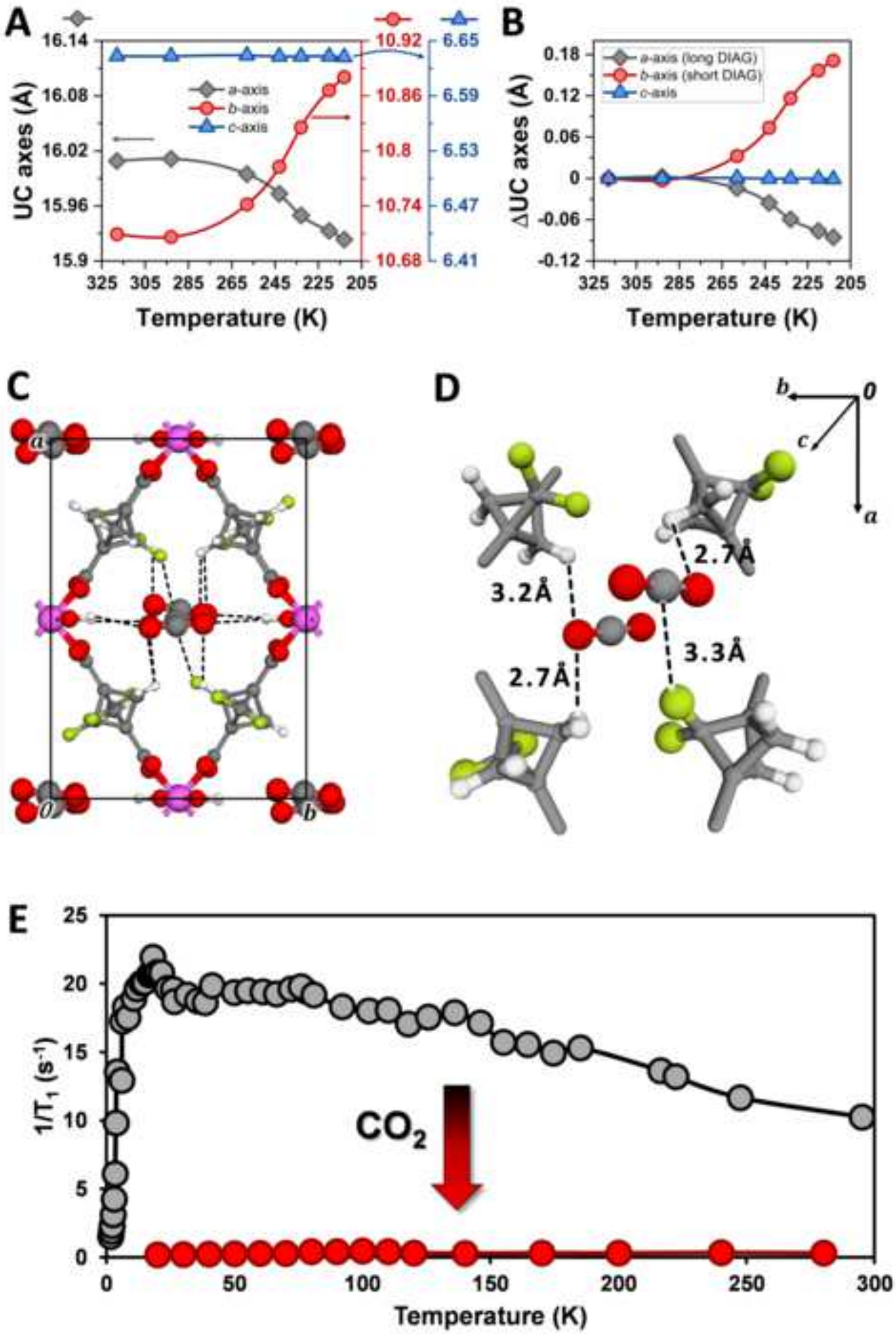

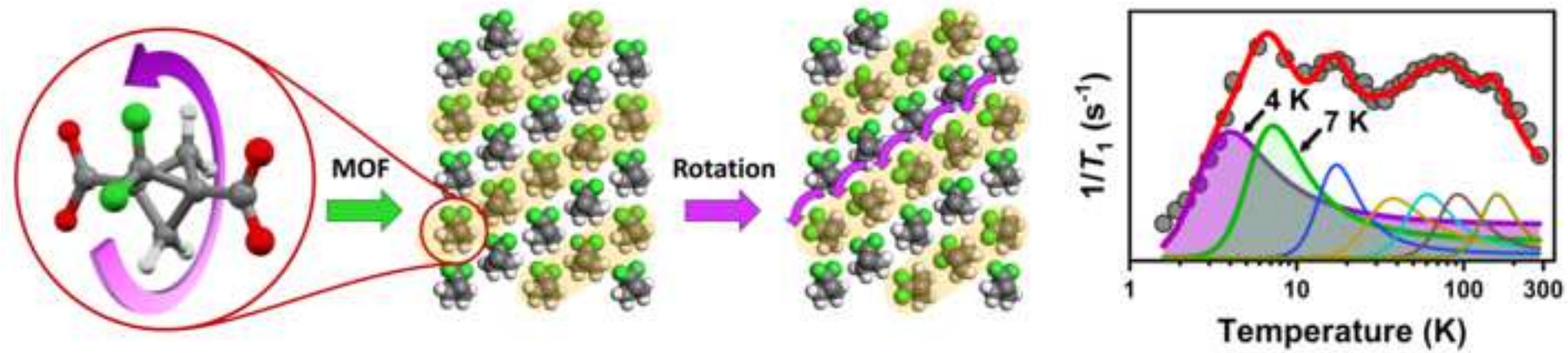
MOF
Rotation
4 K
7 K
1/T1 (s-1)
1
10
100
300
Temperature (K)